

# Uncovering Modality Discrepancy and Generalization Illusion for General-Purpose 3D Medical Segmentation

Yichi Zhang<sup>1,2,\*</sup>, Feiyang Xiao<sup>1,2,\*</sup>, Le Xue<sup>1,2,†</sup>, Wenbo Zhang<sup>1,2</sup>, Gang Feng<sup>1,3</sup>, Chenguang Zheng<sup>1,2</sup>, Yuan Qi<sup>1,2</sup>, Yuan Cheng<sup>1,2,†</sup>, and Zixin Hu<sup>1,2,†</sup>

<sup>1</sup> Fudan University, Shanghai, China.

<sup>2</sup> Shanghai Academy of Artificial Intelligence for Science, Shanghai, China.

<sup>3</sup> Shanghai Universal Medical Imaging Diagnostic Center, Shanghai, China.

**Abstract.** While emerging 3D medical foundation models are envisioned as versatile tools with offer general-purpose capabilities, their validation remains largely confined to regional and structural imaging, leaving a significant modality discrepancy unexplored. To provide a rigorous and objective assessment, we curate the UMD dataset comprising 490 whole-body PET/CT and 464 whole-body PET/MRI scans ( $\sim 675$ k 2D images,  $\sim 12$ k 3D organ annotations) and conduct a thorough and comprehensive evaluation of representative 3D segmentation foundation models. Through intra-subject controlled comparisons of paired scans, we isolate imaging modality as the primary independent variable to evaluate model robustness in real-world applications. Our evaluation reveals a stark discrepancy between literature-reported benchmarks and real-world efficacy, particularly when transitioning from structural to functional domains. Such systemic failures underscore that current 3D foundation models are far from achieving truly general-purpose status, necessitating a paradigm shift toward multi-modal training and evaluation to bridge the gap between idealized benchmarking and comprehensive clinical utility. This dataset and analysis establish a foundational cornerstone for future research to develop truly modality-agnostic medical foundation models: <https://github.com/YichiZhang98/UMD>.

**Keywords:** Medical Image Segmentation · General-Purpose Segmentation · Vision Foundation Model · Volumetric Medical Images

## 1 Introduction

The field of medical image segmentation is undergoing a paradigm shift from task-specific models to general-purpose foundation models [9,15]. Inspired by the success of the Segment Anything Model (SAM) in computer vision [6], there is a burgeoning interest in developing and adapting large-scale pre-trained models in medical scenarios [11,14,19]. However, direct adaptation of natural-image-based models to the medical domain faces significant structural hurdles. A primary limitation is that many existing adaptations operate via 2D slice-wise segmentation [8,17], when adapted to 3D medical images, the volumes are segmented

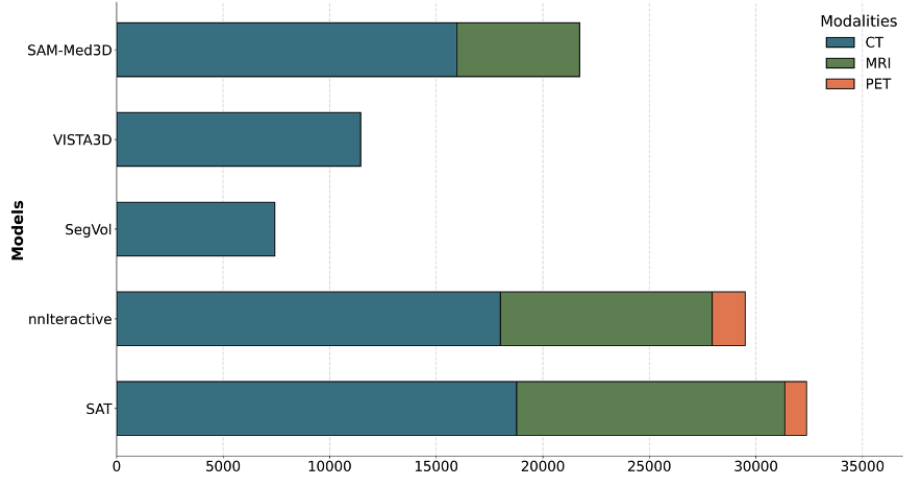


**Fig. 1.** The structural bias in data distribution of general-purpose medical segmentation foundation models. A profound disparity is observed between structural imaging (CT and MRI) and functional imaging (PET), with the latter constituting a negligible fraction of the total data across all models.

slice-by-slice and reconstructed through post-processing. This strategy inherently overlooks the critical volumetric contextual information and inter-slice spatial correlations that are fundamental to radiological interpretation [13].

To address the shortcomings of 2D models, a series of 3D general-purpose medical foundation models have recently emerged [1,4,5,12,18] to leverage intrinsic volumetric features directly and achieve remarkable generalization capabilities across a wide array of 3D segmentation tasks. While these 3D medical foundation models claim to provide a unified solution for diverse clinical tasks, their validation remains largely restricted to structural imaging (See Fig. 1). This leaves a significant modality discrepancy unexplored, particularly the divergence between anatomical structure and functional metabolism [16]. Besides, most existing evaluations rely on test splits from aggregated datasets, overlooking performance under realistic out-of-distribution scenarios. We argue that current models possess a fundamental structural bias originating from their training and validation protocols, leading to an over-optimistic perception of their universality.

To expose the inherent modality discrepancy and the underlying generalization illusion, we constructed a benchmark of 490 paired PET/CT and 464 paired PET/MRI for whole-body segmentation of 13 organs, enabling a direct comparison of model performance across co-registered modalities, as shown in Fig. 2. By utilizing intra-subject controlled comparisons, we effectively isolate imaging modality as the primary independent variable, allowing for a rigorous quantification. Furthermore, our benchmark serves as a pristine testbed to evaluate the

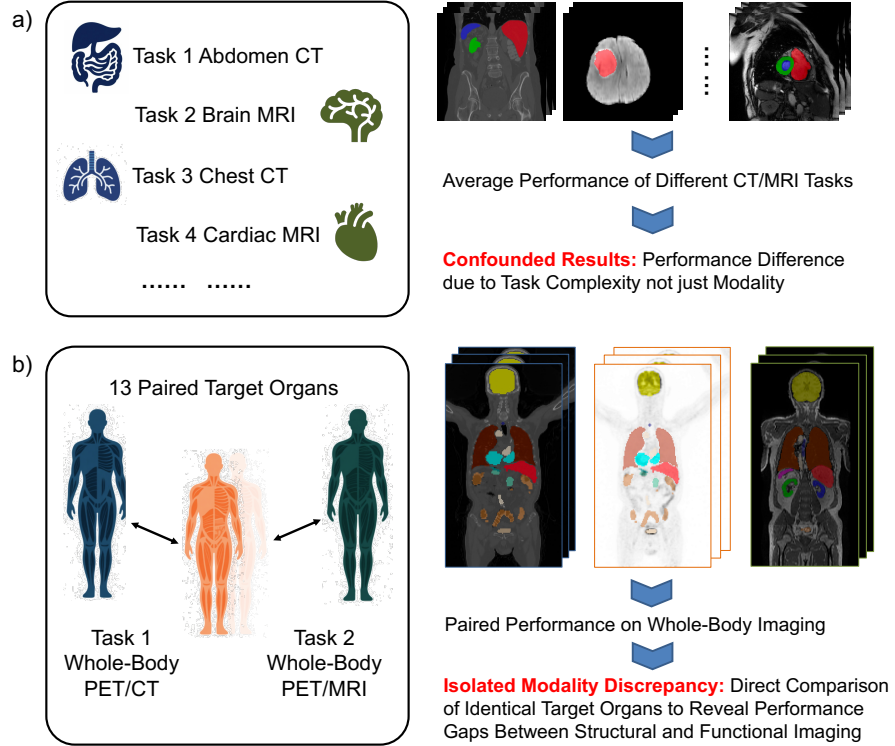


**Fig. 2.** (a) Existing validation protocols typically assess models on heterogeneous datasets where modality is intrinsically entangled with specific anatomical tasks. This approach prevents an isolated measurement of modality-specific robustness, as performance variations are confounded by varying task complexities. (b) In contrast, our evaluation utilizes paired whole-body PET/CT and PET/MRI data. By performing simultaneous segmentation of identical targets across paired structural and functional modalities, we effectively isolates the Modality Discrepancy, enabling a direct and rigorous quantification.

true zero-shot generalization performance of these models on previously unseen data. Our systematic evaluation reveals a stark discrepancy between literature-reported benchmarks and real-world performance, with substantial degradation in effectiveness and, in some cases, complete failure. These findings expose the systemic limitations of current foundation models and underscore the urgent necessity to bridge the gap between idealized benchmarking and comprehensive clinical utility, establishing a foundational cornerstone for the development of truly modality-agnostic medical foundation models.

## 2 Validation Pitfalls

The rapid evolution of general-purpose medical segmentation foundation models has been accompanied by increasing benchmark datasets. However, a critical examination of current validation protocols reveals several pitfalls that obscure the true limits of these models, particularly regarding their robustness across different imaging modalities.

### **The Entanglement of Task Complexity and Modality Discrepancy.**

A primary pitfall in existing evaluations is the inherent entanglement of anatomical task complexity with imaging modality. Most benchmarks utilize disparate datasets for different modalities, such as CT for abdominal organs [10] and MRI for intricate cardiac or neurological structures [7]. Consequently, performance metrics become fundamentally confounded, as it remains impossible to discern whether a performance gap arises from the underlying imaging physics or the intrinsic geometric difficulty of the anatomical target (See Fig. 2a). Furthermore, the reliance on heterogeneous patient cohorts and disjointed acquisition environments introduces significant confounding variables. While limited paired datasets exist [2,3], their frequent inclusion in the pre-training phases of general-purpose models further compromises their utility as objective benchmarks. Without the simultaneous capture of identical structures, the modality gap cannot be isolated as a primary independent variable.

**The Structural Bias in Data Distribution.** Current validation frameworks exhibit a profound morphological bias, focusing almost exclusively on modalities that provide high-contrast physical boundaries (See Fig. 1). This concentration on CT and MRI creates a restricted definition of generalization rooted in anatomical density and geometry. Functional imaging such as PET, represents a significant void in existing evaluations. Unlike structural imaging, PET captures metabolic activity, resulting in signal profiles characterized by diffused edges and lower signal-to-noise ratios [16]. By neglecting functional modalities, current protocols fail to expose the limitations of foundation models in interpreting metabolic-driven signal distributions, leading to an incomplete assessment of true cross-modality robustness.

## 3 Benchmark Design

A significant limitation in current evaluations of general-purpose medical segmentation models is the reliance on heterogeneous datasets, where different modalities often correspond to disparate anatomical regions or clinical tasks. To address the methodological gaps identified in current validation protocols, we propose a controlled experimental framework that isolates modality discrepancy as the primary variable.

To bridge the gap between idealized benchmarking and real-world utility, we construct a novel dataset comprising two subtasks: 490 cases of whole-body PET/CT and 464 cases of whole-body PET/MRI. For each case, the structural (CT or MRI) and functional (PET) volumes were acquired from the same

subject during a single diagnostic session, ensuring intrinsic spatial and anatomical consistency. This intra-subject paired nature guarantees that the underlying morphology, scale, and orientation of the target organs remain constant across modalities. Voxel-wise annotations were provided for 13 diverse organs, including the liver, left kidney, right kidney, brain, heart, spleen, aorta, lung, colon, urinary bladder, pancreas, esophagus, and stomach. By providing ground-truth labels for both structural and functional imaging, our protocol enables a head-to-head comparison between different modalities. Furthermore, as a newly collected dataset rather than a recompilation of existing public sources, we eliminate the risk of data leakage, guaranteeing the validity and authenticity of the evaluation results.

To comprehensively evaluate the robustness of current 3D medical foundation models, we conducted a systematic comparison of five representative state-of-the-art general-purpose segmentation foundation models, including SAM-Med3D-turbo [12], SegVol [1], SAT-Pro [18], VISTA3D [4], and nnInteractive [5]. These models represent the cutting edge of general-purpose segmentation, utilizing diverse strategies such as large-scale pre-training on volumetric data, prompt-based interaction, and universal feature encoders. Notably, each of these frameworks has claimed to achieve superior zero-shot generalization performance across a wide array of 3D medical imaging tasks and anatomical structures.

## 4 Results and Discussion

Table 1 summarizes the segmentation performance of all evaluated models on PET and CT segmentation. A primary observation is the selective paralysis of semantic-guided models, such as VISTA3D and SAT. While VISTA3D demonstrates high precision in segmenting the liver from CT, this success proves to be an isolated outlier rather than a reflection of general-purpose ability. Across nearly all other targets and modalities, these models exhibit a catastrophic failure, with Dice scores frequently plummeting to near-zero. This suggests that their knowledge is not rooted in a deep understanding of human anatomy but is instead overfitted to specific, high-frequency patterns within their training distributions. The total collapse of SAT across both CT and PET further underscores that text-driven prompts are currently insufficient for handling the distribution shifts encountered in real-world clinical benchmarks.

In contrast, models utilizing point-based interactions, such as SAM-Med3D-turbo and nnInteractive, maintain a higher degree of continuity, yet their performance remains far from clinically reliable. These frameworks essentially utilize spatial prompts for localization, allowing them to achieve moderate success in high-contrast regions like the brain or lung. However, their lack of true structural robustness is exposed when dealing with intricate or low-contrast geometries such as the aorta, esophagus, or pancreas, where even with precise point guidance, they fail to delineate boundaries accurately.

By isolating imaging modality as the primary variable, our intra-subject comparison reveals a profound generalization gap between structural CT and func-

**Table 1.** Evaluation results (DSC) of representative general-purpose segmentation foundation models for zero-shot promptable PET and CT segmentation. Results in **red** and **blue** are the performance of **PET** and **CT**, respectively. Light gray and dark gray shaded cells indicate results that are significantly better with  $p < 0.01$  and  $p < 0.0001$ .

Model	SAM-Med3D-tb	SegVol	nnInteractive	VISTA3D	SAT
Liver	0.7039(0.1155)	0.0806(0.1982)	0.4993(0.3319)	0.9186(0.0378)	0.0057(0.0205)
	0.6835(0.1100)	0.1618(0.2539)	0.3904(0.3769)	0.0676(0.0475)	0.0020(0.0451)
Kidney-L	0.4701(0.1300)	0.1203(0.1967)	0.7930(0.1636)	0.0000(0.0000)	0.0001(0.0018)
	0.5678(0.1411)	0.0687(0.1329)	0.4464(0.3436)	0.0000(0.0000)	0.0041(0.0638)
Kidney-R	0.4387(0.1491)	0.1437(0.2279)	0.7780(0.1753)	0.0000(0.0001)	0.0061(0.0780)
	0.5596(0.1843)	0.0630(0.1178)	0.4187(0.3413)	0.0003(0.0020)	0.0082(0.0900)
Brain	0.6760(0.2378)	0.3024(0.3926)	0.7940(0.1432)	0.0000(0.0000)	0.0020(0.0451)
	0.6609(0.3030)	0.1399(0.2408)	0.8796(0.1250)	0.0000(0.0000)	0.0020(0.0451)
Heart	0.5073(0.0992)	0.0993(0.1863)	0.5607(0.2908)	0.0000(0.0000)	0.0020(0.0451)
	0.4581(0.1323)	0.1148(0.1994)	0.2214(0.2641)	0.0001(0.0013)	0.0041(0.0638)
Spleen	0.5110(0.1483)	0.1208(0.2065)	0.6064(0.2937)	0.0000(0.0000)	0.0061(0.0780)
	0.5827(0.1295)	0.1105(0.2000)	0.4378(0.3516)	0.0001(0.0014)	0.0061(0.0780)
Aorta	0.1343(0.0588)	0.0465(0.0900)	0.2356(0.1325)	0.0000(0.0000)	0.0024(0.0452)
	0.1635(0.0600)	0.0541(0.0894)	0.0662(0.0936)	0.0000(0.0000)	0.0020(0.0451)
Lung	0.6243(0.0767)	0.1426(0.2239)	0.4805(0.2361)	0.0002(0.0015)	0.0429(0.0151)
	0.5307(0.1522)	0.0236(0.0594)	0.3345(0.2679)	0.0002(0.0006)	0.0020(0.0451)
Colon	0.1316(0.0838)	0.0384(0.0769)	0.0701(0.0631)	0.0000(0.0000)	0.1465(0.0727)
	0.1298(0.0652)	0.0264(0.0519)	0.0685(0.0792)	0.0000(0.0000)	0.0000(0.0000)
Bladder	0.3960(0.1774)	0.0972(0.1704)	0.5234(0.2486)	0.0000(0.0000)	0.0021(0.0451)
	0.5900(0.2343)	0.1016(0.1950)	0.6676(0.2430)	0.0000(0.0000)	0.0020(0.0451)
Pancreas	0.1233(0.0813)	0.0743(0.1296)	0.4007(0.1399)	0.0000(0.0000)	0.0115(0.0252)
	0.1589(0.0767)	0.0299(0.0594)	0.0844(0.0894)	0.0002(0.0022)	0.0041(0.0638)
Esophagus	0.0904(0.0545)	0.0356(0.0690)	0.1721(0.0867)	0.0000(0.0000)	0.0057(0.0472)
	0.0620(0.0321)	0.0235(0.0416)	0.0749(0.0662)	0.0000(0.0000)	0.0020(0.0451)
Stomach	0.4459(0.1482)	0.0875(0.1680)	0.3536(0.2567)	0.0000(0.0000)	0.0022(0.0036)
	0.1945(0.1477)	0.0546(0.1127)	0.3563(0.3034)	0.0000(0.0000)	0.0041(0.0638)
Avg	0.4035(0.0417)	0.1071(0.1376)	0.4813(0.0737)	0.0706(0.0045)	0.0181(0.0207)
	0.4101(0.5016)	0.0747(0.0971)	0.3416(0.0999)	0.0053(0.0037)	0.0033(0.0440)

tional PET. This systemic failure is only temporarily mitigated in specific organs such as the bladder, where the intense accumulation of radiotracers creates extreme signal contrast in PET. Beyond these high-uptake exceptions, however, the models suffer a catastrophic loss of utility, indicating that current 3D foundation models are fundamentally modality-locked to structural priors and remain incapable of bridging the gap between anatomical density and metabolic activity.

Consistent with the PET/CT results, Table 2 demonstrates a similar pattern on the PET/MRI dataset. While point-prompt models like nnInteractive and SAM-Med3D-turbo achieve slightly higher average scores on structural MRI compared to CT likely benefiting from MRI’s superior soft-tissue contrast in organs such as the liver and brain, this structural proficiency fails to translate into functional robustness. The transition to PET imaging once again triggers a precipitous decline in performance. The total collapse of semantic-guided models is remained in this setting. Consistent with the PET/CT findings, localized performance recoveries in PET are only observed in high-uptake regions.

**Table 2.** Evaluation results (DSC) of representative general-purpose segmentation foundation models for zero-shot promptable PET and MRI segmentation. Results in **red** and **teal** are the performance of **PET** and **MRI**, respectively. Light grey and dark gray shaded cells indicate results that are significantly better with  $p < 0.01$  and  $p < 0.0001$ .

Model	SAM-Med3D-tb	SegVol	nnInteractive	VISTA3D	SAT
Liver	<b>0.7719(0.0755)</b>	0.3986(0.2433)	<b>0.8209(0.2412)</b>	0.0384(0.0548)	0.0000(0.0005)
	<b>0.6259(0.2050)</b>	<b>0.3731(0.2500)</b>	<b>0.1225(0.2252)</b>	<b>0.0749(0.0244)</b>	0.0000(0.0000)
Kidney-L	<b>0.4857(0.1422)</b>	<b>0.1090(0.1136)</b>	<b>0.6346(0.2242)</b>	0.0000(0.0000)	0.0000(0.0000)
	<b>0.5666(0.1142)</b>	<b>0.1047(0.0867)</b>	0.1679(0.2398)	0.0000(0.0000)	0.0000(0.0000)
Kidney-R	<b>0.5521(0.1488)</b>	0.0917(0.1088)	<b>0.7040(0.1546)</b>	0.0000(0.0000)	0.0000(0.0000)
	<b>0.5708(0.1257)</b>	0.0884(0.0785)	<b>0.2225(0.2494)</b>	<b>0.0057(0.0207)</b>	0.0000(0.0000)
Brain	<b>0.5797(0.1767)</b>	0.2342(0.1919)	0.6405(0.3937)	0.0002(0.0010)	<b>0.0378(0.0072)</b>
	<b>0.7707(0.0746)</b>	<b>0.2654(0.2306)</b>	<b>0.7860(0.3120)</b>	0.0000(0.0000)	0.0000(0.0000)
Heart	<b>0.6799(0.0893)</b>	0.0987(0.1069)	<b>0.5633(0.3423)</b>	0.0000(0.0000)	0.0000(0.0000)
	<b>0.6685(0.1012)</b>	<b>0.2382(0.2124)</b>	<b>0.1430(0.2047)</b>	0.0000(0.0000)	0.0000(0.0000)
Spleen	<b>0.5609(0.1130)</b>	<b>0.1564(0.1477)</b>	<b>0.6719(0.2582)</b>	0.0000(0.0000)	0.0000(0.0000)
	<b>0.4353(0.1606)</b>	0.1655(0.1422)	<b>0.1368(0.2115)</b>	0.0000(0.0000)	0.0000(0.0000)
Aorta	<b>0.0709(0.0458)</b>	0.0866(0.0872)	<b>0.2009(0.1384)</b>	0.0000(0.0000)	0.0000(0.0000)
	<b>0.0837(0.0437)</b>	<b>0.1186(0.0811)</b>	0.0465(0.0662)	0.0000(0.0000)	0.0000(0.0000)
Lung	<b>0.6046(0.0938)</b>	0.2611(0.2298)	<b>0.5700(0.1768)</b>	0.0000(0.0000)	<b>0.0005(0.0022)</b>
	<b>0.1892(0.1183)</b>	0.0469(0.0718)	<b>0.2685(0.2484)</b>	<b>0.0002(0.0007)</b>	0.0000(0.0000)
Colon	<b>0.1091(0.0586)</b>	0.0478(0.0648)	<b>0.1115(0.1110)</b>	0.0000(0.0000)	<b>0.0346(0.0556)</b>
	<b>0.1225(0.0661)</b>	<b>0.0416(0.0478)</b>	<b>0.0532(0.0632)</b>	0.0000(0.0000)	0.0000(0.0000)
Bladder	<b>0.6176(0.1912)</b>	0.0452(0.0863)	<b>0.5908(0.2813)</b>	0.0000(0.0000)	0.0000(0.0000)
	<b>0.6548(0.2074)</b>	<b>0.2613(0.2188)</b>	<b>0.5999(0.2067)</b>	0.0000(0.0000)	0.0000(0.0000)
Pancreas	<b>0.1642(0.0834)</b>	0.0579(0.0625)	<b>0.2961(0.1992)</b>	0.0002(0.0025)	0.0043(0.0655)
	<b>0.1702(0.0831)</b>	<b>0.0552(0.0559)</b>	<b>0.0554(0.0732)</b>	0.0000(0.0000)	0.0043(0.0655)
Esophagus	<b>0.0352(0.0209)</b>	<b>0.0837(0.0678)</b>	<b>0.1177(0.0936)</b>	0.0000(0.0000)	0.0000(0.0000)
	<b>0.0335(0.0169)</b>	<b>0.0435(0.0362)</b>	<b>0.0360(0.0448)</b>	0.0000(0.0000)	0.0000(0.0000)
Stomach	<b>0.4073(0.1306)</b>	<b>0.0701(0.0925)</b>	<b>0.7182(0.2040)</b>	0.0000(0.0000)	0.0000(0.0000)
	<b>0.2888(0.1211)</b>	<b>0.1204(0.0967)</b>	<b>0.1825(0.1667)</b>	0.0000(0.0000)	0.0000(0.0000)
Avg	<b>0.4334(0.0395)</b>	<b>0.1340(0.0411)</b>	<b>0.5107(0.0859)</b>	0.0030(0.0042)	<b>0.0059(0.0065)</b>
	<b>0.3974(0.0552)</b>	<b>0.1480(0.0427)</b>	<b>0.2170(0.0766)</b>	<b>0.0062(0.0027)</b>	0.0003(0.0050)

The stark contrast in Table 3 exposes a profound discrepancy between literature reported benchmarks and actual efficacy on the UMD dataset. We trained nnU-Nets on 10 cases of each modality as a reference of task-specific models for comparison. Most models exhibit a significant performance gap compared to their reported benchmarks, indicating that current 3D foundation models are overfitted to curated data distributions and lack the robustness required for diverse clinical scenarios. Specifically, semantic guided models like SAT and VISTA3D undergo a near total collapse upon evaluation on unseen data, revealing that their purported generalization is restricted to specific morphological patterns. This persistent performance gap across all frameworks confirms that structural proficiency does not inherently translate into functional understanding, highlighting a critical limitation in the current foundation model paradigm.

In conclusion, current 3D medical foundation models are **not truly general-purpose**. This limitation has profound implications for their clinical application, as our findings challenge the prevailing narrative that these models possess uni-

**Table 3.** Performance comparison of report average performance of different segmentation tasks from different modalities and paired evaluation performance on proposed UMD benchmark. \* denotes that the test data are different for different models and cannot be directly compared. / denotes that the test data do not contain corresponding modality. ~ denotes that the specific performance for each individual modality is not reported, and only the average performance is presented.

Model	Setting	Reported Performance*			UMD Paired Performance			
		CT	MRI	PET	CT	PET	MRI	PET
SAM-Med3D-tb	1 point	0.790	0.754	/	0.404	0.410	0.433	0.397
SegVol	1 point	0.793	/	/	0.107	0.075	0.134	0.148
nnInteractive	1 point	~0.55	~0.55	/	0.481	0.342	0.511	0.217
VISTA3D	class id	0.711	/	/	0.071	0.005	0.003	0.006
SAT	text	75.6	83.8	63.4	0.018	0.003	0.006	0.000
nnUNet	10 Tr	-	-	-	0.686	0.605	0.652	0.560

versal generalization capabilities. Our study highlights the urgent need to redefine general-purpose in the context of medical imaging to encompass both structural and functional modalities.

While this study provide a rigorous assessment, certain limitations should be acknowledged. Our evaluation primarily focuses on whole-body organs, which do not encompass the complexity of pathological targets. Besides, our current evaluation is restricted to limited prompt types and only utilizes the Dice similarity coefficient for evaluation. However, the substantial performance discrepancies observed across all tested frameworks are sufficiently conclusive to support our core findings regarding the structural bias of current models. Future investigations will explore a broader range of prompting strategies and incorporate diverse evaluation metrics to provide a more granular understanding of model behavior across the entire imaging spectrum.

## 5 Conclusion

This study addresses the critical gap in 3D medical foundation models by curating an intra-subject paired benchmark of 490 PET/CT and 464 PET/MRI scans. By isolating imaging modality as the primary independent variable, we provide a rigorous assessment of model robustness across the structural-functional divide. Our analysis reveals that current foundation models are not truly general-purpose, exhibiting a systemic structural bias that leads to catastrophic performance failure in functional domains. Despite high reported benchmarks, these models remain limited generalization ability in unseen data distributions. By highlighting the critical gap between idealized benchmarking and real-world clinical utility, this study provides a valuable benchmark and insights to guide future advancements in medical foundation models, which we believe will further facilitate collaborative research to develop robust, clinically applicable general-purpose medical AI systems.

## References

1. Du, Y., Bai, F., Huang, T., Zhao, B.: Segvol: Universal and interactive volumetric medical image segmentation. *Advances in neural Information Processing Systems* **37**, 110746–110783. (2024) [2](#), [5](#)
2. Gatidis, S., Früh, M., Fabritius, M.P., Gu, S., Nikolaou, K., Fougère, C.L., Ye, J., He, J., Peng, Y., Bi, L., et al.: Results from the autopet challenge on fully automated lesion segmentation in oncologic pet/ct imaging. *Nature Machine Intelligence* pp. 1–10 (2024) [4](#)
3. Gatidis, S., Hepp, T., Früh, M., La Fougère, C., Nikolaou, K., Pfannenberg, C., Schölkopf, B., Küstner, T., Cyran, C., Rubin, D.: A whole-body fdg-pet/ct dataset with manually annotated tumor lesions. *Scientific Data* **9**(1), 601 (2022) [4](#)
4. He, Y., Guo, P., Tang, Y., Myronenko, A., Nath, V., Xu, Z., Yang, D., Zhao, C., Simon, B., Belue, M., et al.: Vista3d: A unified segmentation foundation model for 3d medical imaging. In: *Proceedings of the Computer Vision and Pattern Recognition Conference*. pp. 20863–20873 (2025) [2](#), [5](#)
5. Isensee, F., Rokuss, M., Krämer, L., Dinkelacker, S., Ravindran, A., Stritzke, F., Hamm, B., Wald, T., Langenberg, M., Ulrich, C., et al.: nninteractive: Redefining 3d promptable segmentation. *arXiv preprint arXiv:2503.08373* (2025) [2](#), [5](#)
6. Kirillov, A., Mintun, E., Ravi, N., Mao, H., Rolland, C., Gustafson, L., Xiao, T., Whitehead, S., Berg, A.C., Lo, W.Y., et al.: Segment anything. In: *Proceedings of the IEEE/CVF international conference on computer vision*. pp. 4015–4026 (2023) [1](#)
7. Lalande, A., Chen, Z., Pommier, T., Decourselle, T., Qayyum, A., Salomon, M., Ginhac, D., Skandarani, Y., Boucher, A., Brahim, K., et al.: Deep learning methods for automatic evaluation of delayed enhancement-mri. the results of the emidec challenge. *Medical Image Analysis* **79**, 102428 (2022) [4](#)
8. Ma, J., He, Y., Li, F., Han, L., You, C., Wang, B.: Segment anything in medical images. *Nature Communications* **15**, 1–9 (2024) [1](#)
9. Ma, J., Wang, B.: Towards foundation models of biological image segmentation. *Nature Methods* **20**(7), 953–955 (2023) [1](#)
10. Ma, J., Zhang, Y., Gu, S., Zhu, C., Ge, C., Zhang, Y., An, X., Wang, C., Wang, Q., Liu, X., Cao, S., Zhang, Q., Liu, S., Wang, Y., Li, Y., He, J., Yang, X.: Abdomenct-1k: Is abdominal organ segmentation a solved problem? *IEEE Transactions on Pattern Analysis and Machine Intelligence* **44**(10), 6695–6714 (2022) [4](#)
11. Mazurowski, M.A., Dong, H., Gu, H., Yang, J., Konz, N., Zhang, Y.: Segment anything model for medical image analysis: an experimental study. *Medical Image Analysis* **89**, 102918 (2023) [1](#)
12. Wang, H., Guo, S., Ye, J., Deng, Z., Cheng, J., Li, T., Chen, J., Su, Y., Huang, Z., Shen, Y., et al.: Sam-med3d: a vision foundation model for general-purpose segmentation on volumetric medical images. *IEEE Transactions on Neural Networks and Learning Systems* (2025) [2](#), [5](#)
13. Zhang, Y., Liao, Q., Ding, L., Zhang, J.: Bridging 2d and 3d segmentation networks for computation-efficient volumetric medical image segmentation: An empirical study of 2.5 d solutions. *Computerized Medical Imaging and Graphics* p. 102088 (2022) [2](#)
14. Zhang, Y., Lv, B., Xue, L., Zhang, W., Liu, Y., Fu, Y., Cheng, Y., Qi, Y.: Semisam+: Rethinking semi-supervised medical image segmentation in the era of foundation models. *Medical Image Analysis* **106**, 103733 (2025) [1](#)

15. Zhang, Y., Shen, Z., Jiao, R.: Segment anything model for medical image segmentation: Current applications and future directions. *Computers in Biology and Medicine* p. 108238 (2024) [1](#)
16. Zhang, Y., Xue, L., Zhang, W., Li, L., Liu, Y., Jiang, C., Cheng, Y., Qi, Y.: Seganypet: Universal promptable segmentation from positron emission tomography images. In: *Proceedings of the IEEE/CVF International Conference on Computer Vision (ICCV)*. pp. 21107–21116 (2025) [2](#), [4](#)
17. Zhao, T., Gu, Y., Yang, J., Usuyama, N., Lee, H.H., Kiblawi, S., Naumann, T., Gao, J., Crabtree, A., Abel, J., et al.: A foundation model for joint segmentation, detection and recognition of biomedical objects across nine modalities. *Nature methods* **22**(1), 166–176 (2025) [1](#)
18. Zhao, Z., Zhang, Y., Wu, C., Zhang, X., Zhou, X., Zhang, Y., Wang, Y., Xie, W.: Large-vocabulary segmentation for medical images with text prompts. *NPJ Digital Medicine* **8**(1), 566 (2025) [2](#), [5](#)
19. Zhou, N., Zou, K., Ren, K., Luo, M., He, L., Wang, M., Chen, Y., Zhang, Y., Chen, H., Fu, H.: Medsam-u: Uncertainty-guided auto multi-prompt adaptation for reliable medsam. *IEEE Transactions on Circuits and Systems for Video Technology* (2025) [1](#)

## Appendix

### Dataset Collection

In this study, we retrospectively collected 490 whole-body PET/CT and 464 whole-body PET/MRI scans. The PET/CT imaging was conducted using a Siemens Biograph 64 scanner. Patients fasted for at least 6 hours with blood glucose levels confirmed at  $< 11.1$  mmol/L prior to receiving an intravenous injection of  $^{18}\text{F}$ -FDG. PET/MRI data were acquired using a 3.0T Siemens Biograph mMR system. Patients fasted for at least 6 hours and serum glucose levels were confirmed prior to the  $^{18}\text{F}$ -FDG injection. The scanning field was from the midthigh level to the top of head with the subject in the supine position.

### Implementation Details

To ensure a fair and rigorous evaluation, we utilized the official, latest, and largest-scale pre-trained weights and codebases for all comparing foundation models. All experiments were conducted on an NVIDIA A100 GPU with 80GB of memory. Following the standardized evaluation protocols associated with each model, we implemented two primary interaction strategies to facilitate zero-shot segmentation. For VISTA3D and SAT, we provided the specific textual category or class ID corresponding to each of the target organs. For other point-based models, we utilized simulated point prompts generated from the ground truth masks to mimic ideal user interaction.

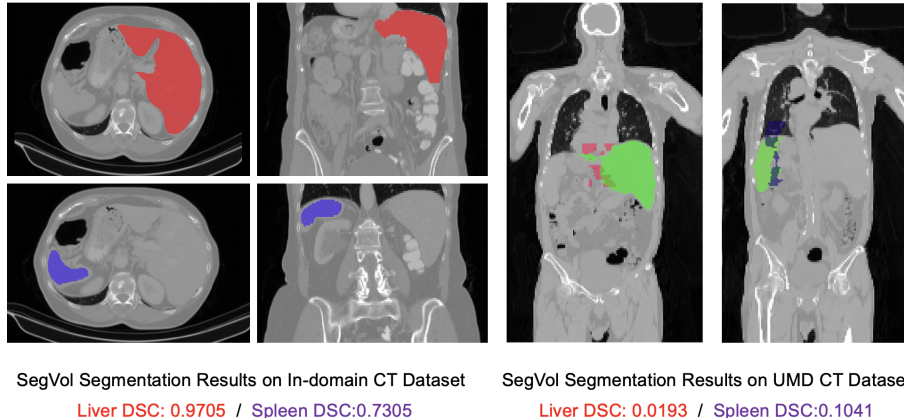


**Fig. 3.** Visual comparison of failure cases of SegVol with performance across in-domain and out-of-domain UMD datasets. This stark illustrates the **generalization illusion**, where high scores on benchmark datasets fail to translate into robust clinical utility on unseen distributions.

### Visual Comparison and Analysis

The visual evidence in Fig. 3 provides a concrete manifestation of the generalization illusion discussed in our study. While SegVol demonstrates near-radiologist-level precision on in-domain data, its performance undergoes a systemic collapse when applied to the UMD CT dataset. The fragmented segmentation of the liver and spleen on the UMD benchmark suggests that the model is heavily overfitted to specific intensity distributions and morphological priors of its training corpus. This failure occurs even within the structural CT domain before any transition to functional PET imaging. This reveals that many foundation models are highly sensitive to subtle shifts in acquisition parameters or patient cohorts.

The intra-subject qualitative assessment in Fig. 4 provides a critical visual testament to the modality-induced generalization gap. Even though nnInteractive maintains the most consistent scores among all tested foundation models, its transition from structural to functional imaging reveals a stark limitation. While it achieves a moderate performance on the CT modality, this performance is significantly decreased when applied to PET modality. This suggests that the model’s feature space is fundamentally anchored to structural intensity profiles.

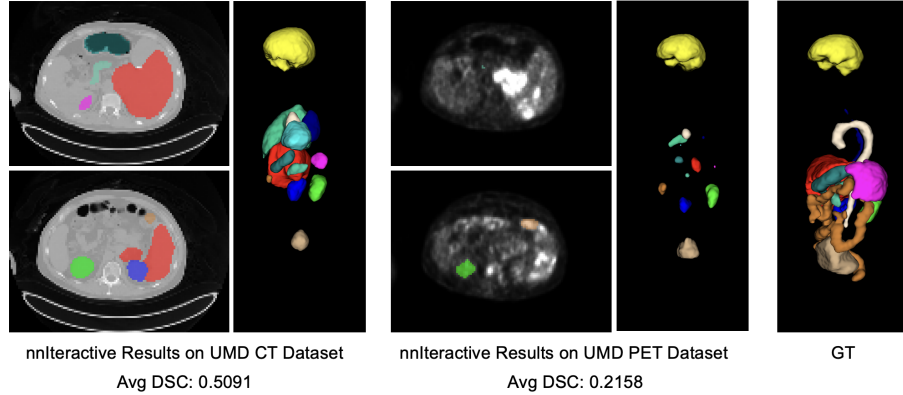


**Fig. 4.** Qualitative assessment of **modality discrepancy** via nnInteractive underscores a fundamental performance gap. Despite exhibiting the highest relative generalization ability in our evaluation, the model remains incapable of mapping anatomical priors onto the distinct signal profiles of metabolic imaging.